Inorg. Chem. **2004**, *43*, 1056–1064

Stepwise Synthesis of $[Ru(trpy)(L)(X)]^{n+}$ (trpy = 2,2′:6′,2″-Terpyridine; L = 2,2′-Dipyridylamine; X = Cl^-, H_2O, NO_2^-, NO^+, O^{2-}). Crystal Structure, Spectral, Electron-Transfer, and Photophysical Aspects

Nripen Chanda,[†] Shaikh M. Mobin,[†] Vedavati G. Puranik,[‡] Anindya Datta,[†] Mark Niemeyer,[§] and Goutam Kumar Lahiri*,[†]

Department of Chemistry, Indian Institute of Technology—Bombay, Powai, Mumbai 400076, India, Physical Chemistry Division, National Chemical Laboratory, Pune, Maharashtra 411008, India, and Institut für Anorganische Chemie, Universität Stuttgart, Pfaffenwaldring 55, D-70569 Stuttgart, Germany

Received July 30, 2003

Ruthenium–terpyridine complexes incorporating a 2,2′-dipyridylamine ancillary ligand $[Ru^{II}(trpy)(L)(X)](ClO_4)_n$ [trpy = 2,2′:6′,2″-terpyridine; L = 2,2′-dipyridylamine; and X = Cl^-, $n = 1$ (**1**); X = H_2O, $n = 2$ (**2**); X = NO_2^-, $n = 1$ (**3**); X = NO^+, $n = 3$ (**4**)] were synthesized in a stepwise manner starting from $Ru^{III}(trpy)(Cl)_3$. The single-crystal X-ray structures of all of the four members (**1**–**4**) were determined. The Ru(III)/Ru(II) couple of **1** and **3** appeared at 0.64 and 0.88 V versus the saturated calomel electrode in acetonitrile. The aqua complex **2** exhibited a metal-based couple at 0.48 V in water, and the potential increased linearly with the decrease in pH. The electron–proton content of the redox process over the pH range of 6.8–1.0 was calculated to be a $2e^-/1H^+$ process. However, the chemical oxidation of **2** by an aq Ce(IV) solution in 1 N H_2SO_4 led to the direct formation of corresponding oxo species $[Ru^{IV}(trpy)(L)(O)]^{2+}$ via the concerted $2e^-/2H^+$ oxidation process. The two successive reductions of the coordinated nitrosyl function of **4** appeared at +0.34 and –0.34 V corresponding to $Ru^{II}–NO^+ \rightarrow Ru^{II}–NO^\bullet$ and $Ru^{II}–NO^\bullet \rightarrow Ru^{II}–NO^-$, respectively. The one-electron-reduced $Ru^{II}–NO^\bullet$ species exhibited a free-radical electron paramagnetic resonance signal at $g = 1.990$ with nitrogen hyperfine structures at 77 K. The NO stretching frequency of **4** (1945 cm^{-1}) was shifted to 1830 cm^{-1} in the case of $[Ru^{II}(trpy)(L)(NO^\bullet)]^{2+}$. In aqueous solution, the nitrosyl complex **4** slowly transformed to the nitro derivative **3** with the pseudo-first-order rate constant of $k_{298}/s^{-1} = 1.7 \times 10^{-4}$. The chloro complex **1** exhibited a dual luminescence at 650 and 715 nm with excited-state lifetimes of 6 and 1 μs, respectively.

Introduction

The relevance of nitric oxide (NO) in a wide range of biological[1] and environmental processes[2] and, in particular, its applications in the form of ruthenium nitrosyl complexes as antitumor and antiseptic agents[3] have introduced a renewed interest in developing newer classes of ruthenium nitrosyls. The unique redox noninnocent behavior of the coordinated NO molecule makes it susceptible to shuttling between the possible redox states NO^+, NO, and NO^-, depending on the ancillary functionalities in the complex molecules. For example, in metmyoglobin, the iron center binds with the NO as $Fe^{II}–NO^+$,[4] and in reduced vitamin B_{12}, the cobalt center binds with the NO in the form of $Co^{III}–NO^-$.[5] Moreover, the electrophilicity of the $M–NO^+$ center ($\nu_{NO} > 1900$ cm^{-1}) draws special attention because the coordi-

* Author to whom correspondence should be addressed. E-mail: lahiri@chem.iitb.ac.in.
[†] Indian Institute of Technology—Bombay.
[‡] National Chemistry Laboratory.
[§] Universität Stuttgart.

(1) (a) Howard, J. B.; Rees, D. C. *Chem. Rev.* **1996**, *96*, 2965. (b) Burgees, B. K.; Lowe, D. J. *Chem. Rev.* **1996**, *96*, 2983. (c) Eady, R. R. *Chem. Rev.* **1996**, *96*, 3013. (d) Stamler, J. S.; Singel, D. J.; Loscalzo, J. *Science* **1992**, *258*, 1898. (e) Pfeiffer, S.; Mayer, B.; Hemmens, B. *Angew. Chem., Int. Ed.* **1999**, *38*, 1714. (f) Lang, D. R.; Davis, J. A.; Lopes, L. G. F.; Ferro, A. A.; Vasconcellos, L. C. G.; Franco, D. W.; Tfouni, E.; Wieraszko, A.; Clarke, M. J. *Inorg. Chem.* **2000**, *39*, 2294. (g) Richter-Addo, G. B.; Legzdins, P.; Burstyn, J. C*hem. Rev.* **2002**, *102*, 4. (h) Moncada, S.; Palmer, R. M. J.; Higgs, E. A. *Pharmacol. Rev.* **1991**, *43*, 109. (i) Ritcher-Addo, G. B.; Legzdins, P. *Metal Nitrosyls*; Oxford University Press: New York, 1992. (j) Scheidt, W. R.; Ellison, M. K. *Acc. Chem. Res.* **1999**, *32*, 350. (k) Cooper, C. E. *Biochim. Biophys. Acta* **1999**, *1411*, 290. (l) Wieraszko, A.; Clarke, M. J.; Lang, D. R.; Lopes, L. G. F.; Franco, D. W. *Life Sci.* **2001**, *68*, 1535.

10.1021/ic034902n CCC: $27.50
Published on Web 12/25/2003

nated electrophilic NO^+ is susceptible to undergoing a variety of molecular transformations during nucleophilic attack.[6] A wide variation of electrophilicity of the coordinated Ru−NO^+ moiety has been indeed observed, depending on the electronic aspects of the ancillary ligands present in the complex matrixes. For example, the ν_{NO^+} frequency systematically increases with the increase in the π acidity of the ancillary ligands (L) in a specified complex environment of [Ru(trpy)(L)NO] (trpy = 2,2′:6′,2″-terpyridine and L = 2-phenylpyridine, 1858 cm^{-1};[7] acetylacetonate, 1914 cm^{-1};[8] 2,2′-bipyridine, 1952 cm^{-1};[9] 2-(phenylazo)pyridine, 1960 cm^{-1}).[10] The observed effect of ancillary functionalities in the [(trpy)Ru−NO] core has initiated the present program of the selective introduction of 2,2′-dipyridylamine, which contains a dissociable amine proton and tends to form a nonplanar six-membered chelate ring during the coordination to a metal ion.[11]

The present paper describes a systematic approach of stepwise synthesis of the complexes $[Ru^{II}(trpy)(L)(Cl)](ClO_4)$ (**1**), $[Ru^{II}(trpy)(L)(H_2O)](ClO_4)_2$ (**2**), $[Ru^{II}(trpy)(L)(NO_2)](ClO_4)$ (**3**), and $[Ru^{II}(trpy)(L)(NO)](ClO_4)_3$ (**4**), including the single-crystal X-ray structures of all of the four members (**1**−**4**). The spectroelectrochemical properties of the complexes and photophysical aspects of the starting chloro derivative **1** are also reported. The effectiveness of dipyridylamine as an ancillary ligand in the $[(trpy)Ru^{II}NO]$ core particularly in comparison to the related complexes,[7−10] having ancillary ligands of a different electronic nature, is deliberated.

Results and Discussion

The complexes **1**−**4** were synthesized in a sequential manner from the starting complex $[Ru(trpy)Cl_3]$ as summarized in Scheme 1.

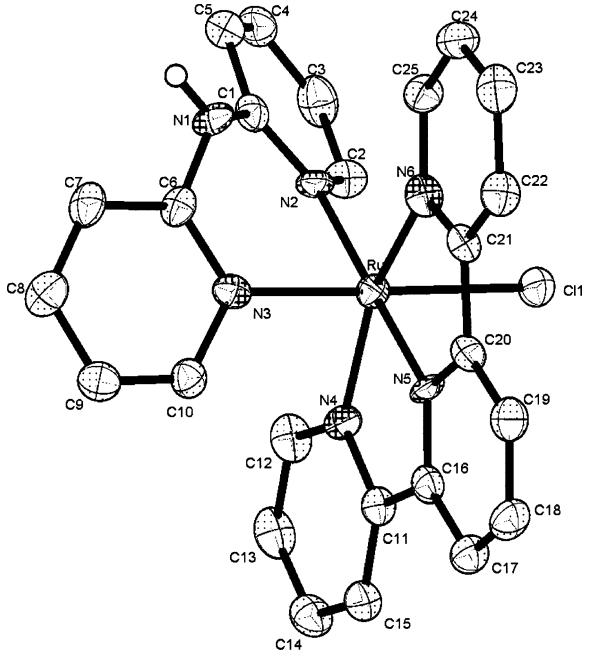

Figure 1. Oak Ridge thermal ellipsoid plot (ORTEP) diagram of **1**. Perchlorate anion is removed for clarity. Ellipsoids are drawn at 50% probability.

Scheme 1

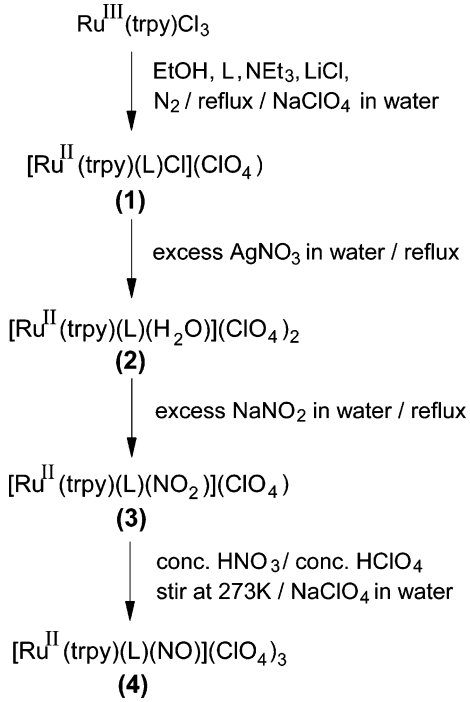

The single-crystal X-ray structures of **1**−**4** are shown in Figures 1−4, respectively. Selected bond distances and angles are set in Table 1, and important crystallographic data are summarized in Table 2. In the complexes, the terpyridine ligand is coordinated to the ruthenium ion in the expected meridional fashion,[12] with the ligand L being in the cis orientation. The geometrical constraint imposed on the

(2) (a) Pandey, K. K. *Coord. Chem. Rev.* **1983**, *51*, 69. (b) Zang, V.; van Eldik, R. *Inorg. Chem.* **1990**, *29*, 4462. (c) Pham, E. K.; Chang, S. G. *Nature* **1994**, *369*, 139.
(3) (a) Fricker, S. P.; Slade, E.; Powell, N. A.; Vaughn, O. J.; Henderson, G. R.; Murrer, S. A.; Megson, I. C.; Bisland, S. K.; Flitney, F. W. *Br. J. Pharmacol.* **1997**, *122*, 1441. (b) Bettache, N.; Carter, T.; Corrie, J. E. T.; Ogden, D.; Trentham, D. R. In *Methods in Enzymology*; Packer, L., Ed.; Academic Press: San Diego, CA, 1996; Vol. 268, p 266. (c) Davies, N.; Wilson, M. T.; Slade, E.; Fricker, S. P.; Murrer, B. A.; Powell, N. A.; Henderson, G. R. *J. Chem. Soc., Chem. Commun.* **1997**, 47. (d) Chen, Y.; Shepherd, R. E. *J. Inorg. Biochem.* **1997**, *68*, 183. (e) Slocik, J. M.; Ward, M. S.; Shepherd, R. E. *Inorg. Chim. Acta* **2001**, *317*, 290. (f) Lopes, L. G. F.; Wieraszko, A.; El-Sherif, Y.; Clarke, M. J. *Inorg. Chim. Acta* **2001**, *312*, 15. (g) Bezerra, C. W. B.; Silva, S. C.; Gambardella, M. T. P.; Santos, R. H. A.; Plicas, L. M. A.; Tfouni, E.; Franco, D. W. *Inorg. Chem.* **1999**, *38*, 5660. (h) Hui, J. W.-S.; Wong, W.-T. *Coord. Chem. Rev.* **1998**, *172*, 389. (i) Lee, S.-M.; Wong, W.-T. *Coord. Chem. Rev.* **1997**, *164*, 415.
(4) Laverman, L. E.; Wanat, A.; Oszajca, J.; Stochel, G.; Ford, P. C.; van Eldik, R. *J. Am. Chem. Soc.* **2001**, *123*, 285.
(5) Wolak, M.; Stochel, G.; Zahl, A.; Schneppensieper, T.; van Eldik, R. *J. Am. Chem. Soc.* **2001**, *123*, 9780.
(6) (a) McCleverty, J. A. *Chem. Rev.* **1979**, *79*, 53. (b) Das, A.; Jones, C. J.; McCleverty, J. A. *Polyhedron* **1993**, *12*, 327. (c) Thiemens, M. H.; Trogler, W. C. *Science* **1991**, *251*, 932. (d) Feelisch, M., Stamler, J. S., Eds.; *Methods in Nitric Oxide Research*; Wiley: Chichester, England, 1996. (e) Enemark, J. H.; Felthan, R. D. *Coord. Chem. Rev.* **1974**, *13*, 339.
(7) Hadadzadeh, H.; DeRosa, M. C.; Yap, G. P. A.; Rezvani, A. R.; Crutchley, R. J. *Inorg. Chem.* **2002**, *41*, 6521.
(8) Dovletoglou, A.; Adeyemi, S. A.; Meyer, T. J. *Inorg. Chem.* **1996**, *35*, 4120.
(9) Pipes, D. W.; Meyer, T. J. *Inorg. Chem.* **1984**, *23*, 2466.
(10) Mondal, B.; Paul, H.; Puranik, V. G.; Lahiri, G. K. *J. Chem. Soc., Dalton Trans.* **2001**, 481.
(11) Chanda, N.; Sarkar, B.; Fiedler, J.; Kaim, W.; Lahiri, G. K. *Dalton Trans.* **2003**, 3550.

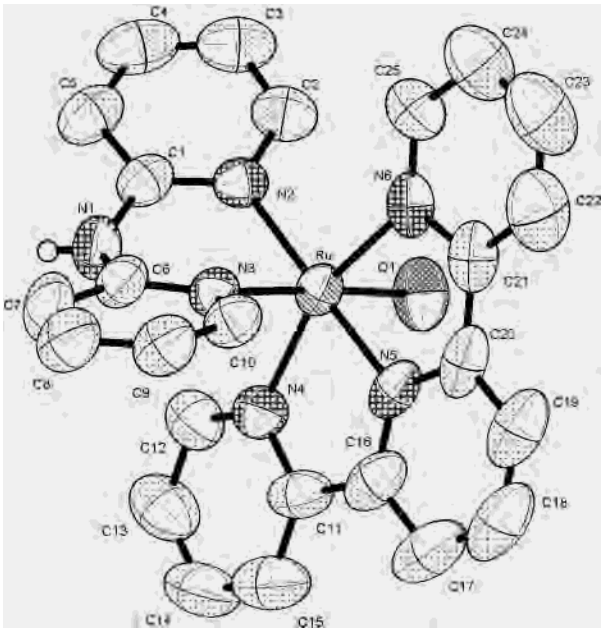

Figure 2. ORTEP diagram of **2**·0.25H_2O. Perchlorate anions and the solvent are removed for clarity. Ellipsoids are drawn at 50% probability.

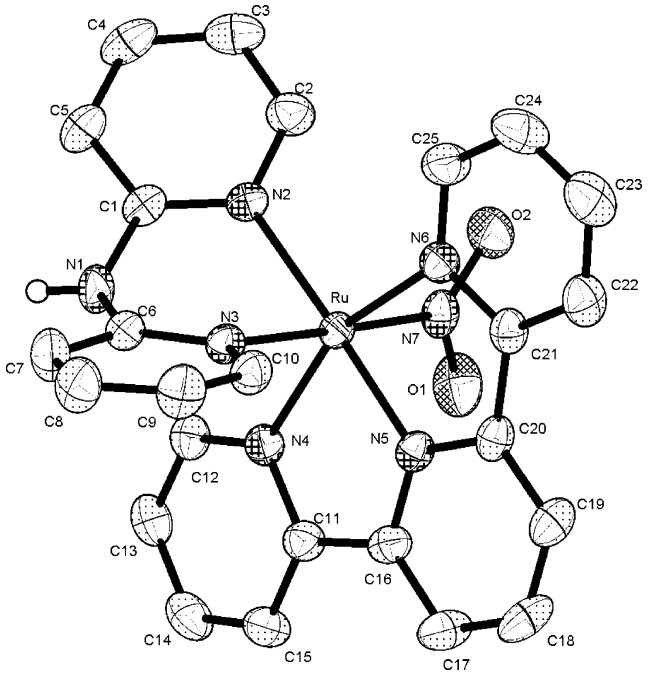

Figure 3. ORTEP diagram of **3**. Perchlorate anion is removed for clarity. Ellipsoids are drawn at 50% probability.

meridional disposition of the terpyridine ligand is reflected in the trans angles, N4−Ru−N6, 159.1(2), 159.2(2), 158.82(9), and 158.5(5)° for **1**−**4**, respectively. The Ru−N5 (central pyridyl nitrogen of terpyridine) distances in the complexes are approximately 0.1 Å shorter than the terminal

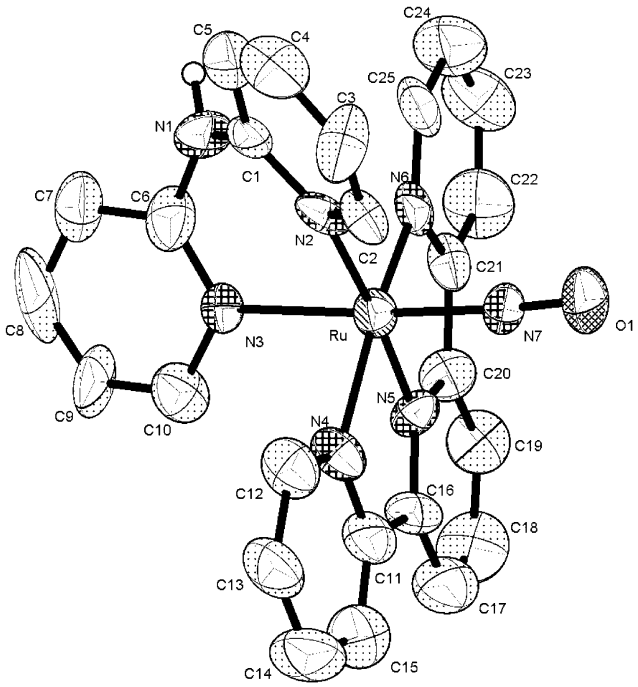

Figure 4. ORTEP diagram of **4**·CH_3CN·0.5H_2O. Perchlorate anions and the solvents are removed for clarity. Ellipsoids are drawn at 50% probability.

Table 1. Selected Bond Distances (Å) and Angles (deg) for **1**−**4**

bond length/ bond angle	**1** (X = Cl)	**2** (X = O1)	**3** (X = N7)	**4** (X = N7)
Ru−X	2.4308(19)	2.126(4)	2.034(2)	1.765(12)
Ru−N2	2.116(6)	2.104(4)	2.128(2)	2.069(11)
Ru−N3	2.060(6)	2.051(4)	2.106(2)	2.096(11)
Ru−N4	2.067(7)	2.090(5)	2.081(2)	2.080(12)
Ru−N5	1.976(5)	1.975(4)	1.970(2)	1.994(11)
Ru−N6	2.089(6)	2.091(5)	2.092(2)	2.113(13)
N7−O1			1.244(3)	1.126(14)
N7−O2			1.257(3)	
N3−Ru−X	177.49(16)	175.38(17)	177.74(9)	176.4(5)
N4−Ru−N6	159.1(2)	159.2(2)	158.82(9)	158.5(5)
N5−Ru−N2	178.6(2)	179.10(18)	177.85(9)	175.8(5)
N5−Ru−N3	94.7(2)	92.83(17)	94.36(9)	89.6(5)
N5−Ru−N4	79.6(2)	79.6(2)	79.41(9)	79.9(5)
N3−Ru−N4	90.5(2)	89.31(17)	90.32(9)	88.8(5)
N5−Ru−N6	79.5(3)	79.6(2)	79.41(9)	79.3(5)
N3−Ru−N6	91.2(2)	93.63(17)	91.09(9)	86.0(4)
N3−Ru−N2	84.9(2)	87.96(17)	83.74(9)	86.8(5)
N4−Ru−N2	101.7(2)	100.81(17)	99.58(9)	98.0(5)
N6−Ru−N2	99.2(2)	99.89(18)	101.58(9)	102.5(5)
N5−Ru−X	87.7(16)	87.86(19)	87.71(9)	92.9(5)
N4−Ru−X	89.37(16)	86.32(18)	89.19(9)	94.3(5)
N6−Ru−X	89.85(16)	91.00(18)	90.17(10)	91.8(5)
N2−Ru−X	92.66(16)	91.38(19)	94.18(9)	90.9(5)
Ru−N7−O1			121.4(2)	176.2(12)
Ru−N7−O2			121.7(2)	
O1−N7−O2			116.9(3)	

Ru−N distances, which in turn maintain the trpy bite angle of ∼79°, typically observed in the terpyridine complexes.[12]

Dipyridylamine ligand is bound to the ruthenium ion with the two pyridine nitrogen donor centers (N2 and N3) having a bite angle of >80°. The coordinated dipyridylamine ligand is nonplanar, in which the two pyridine rings are mutually bent by 45.6(3), 33.2(2), 48.2(1), and 35.6(7)° for **1**−**4**, respectively. To the best of our knowledge, the present set of complexes are the first example of structurally characterized ruthenium−2,2′-dipyridylamine systems, where the

(12) (a) Mondal, B.; Chakraborty, S.; Munshi, P.; Walawalkar, M. G.; Lahiri, G. K. *J. Chem. Soc., Dalton Trans.* **2000**, 2327. (b) Catalano, V. J.; Heck, R. A.; Immoos, C. E.; Ohman, A.; Hill, M. G. *Inorg. Chem.* **1998**, *37*, 2150. (c) Catalano, V. J.; Heck, R. A.; Ohman, A.; Hill, M. G. *Polyhedron* **2000**, *19*, 1049. (d) Mondal, B.; Puranik, V. G.; Lahiri, G. K. *Inorg. Chem.* **2002**, *41*, 5831. (e) Gerli, A.; Reedijk, J.; Lakin, M. T.; Spek, A. L. *Inorg. Chem.* **1995**, *34*, 1836.

Table 2. Crystallographic Data for **1**−**4**

molecular formula	$C_{25}H_{20}Cl_2N_6O_4Ru$ (**1**)	$C_{25}H_{22}Cl_2N_6O_9Ru\cdot0.25H_2O$ (**2**)	$C_{25}H_{20}ClN_7O_6Ru$ (**3**)	$C_{25}H_{20}Cl_3N_7O_{13}Ru\cdot CH_3CN\cdot0.5H_2O$ (**4**)
formula weight	640.44	730.96	651	883.96
radiation	Mo Kα	Mo Kα	Mo Kα	Mo Kα
crystal symmetry	monoclinic	triclinic	monoclinic	orthorhombic
space group	$P2_1/c$	$P\bar{1}$	$P2_1/n$	$Pna2_1$
a (Å)	12.537(4)	9.917(6)	12.6010(11)	18.280(2)
b (Å)	14.545(5)	10.452(6)	14.9180(9)	14.707(1)
c (Å)	14.499(7)	15.431(9)	14.360(2)	12.717(1)
α (deg)	90.0	83.564(9)	90.0	90.0
β (deg)	114.98(3)	75.212(9)	115.326(9)	90.0
γ (deg)	90.0	67.069(9)	90.0	90.0
V (Å^3)	2396.6(16)	1424.1(14)	2440.0(4)	3418.9(6)
Z	4	2	4	4
μ (mm^{-1})	0.925	0.804	0.812	0.772
T (K)	173(2)	293(2)	293(2)	293(2)
D_{calcd} (g cm^{-3})	1.775	1.702	1.772	1.717
2θ range (deg)	3.58−52	4.24−50	3.6−49.84	3.54−49.84
e data (R_{int})	4625 (0.082)	5002 (0.0278)	3960 (0.000)	2585 (0.000)
R1 ($I > 2\sigma(I)$)	0.0685	0.0571	0.0262	0.0563
wR2 (all data)	0.1786	0.1577	0.0623	0.1273
GOF	1.234	1.068	1.058	1.098

dipyridylamine ligand functions as a terminal bidentate ligand. Only one structurally characterized diruthenium complex, encompassing the bridging dipyridylamine ligand, has been reported so far.[13] However, the nonplanarity of the coordinated terminal dipyridylamine ligand was evidenced previously in other structurally characterized metal complexes.[14]

The Ru(II)−Cl distance of 2.4308(19) Å in **1** is slightly longer than that found in [Ru(trpy)(biq)Cl]PF_6 [biq = 2,2′-biquinoline, 2.378(2) Å][15] but is in agreement with those observed in similar complexes.[12]

The single crystal of **2** contains water of crystallization in the ratio **2**:H_2O = 1:0.25. The Ru^{II}−O1(H_2O) bond distance of 2.126(4) Å in **2** is similar to those found in other known Ru^{II}−O(H_2O) structures {[Ru^{II}(trpy)(2-phenylazopyridine)(H_2O)](ClO_4)$_2$, 2.140(5) Å;[16] and [Ru^{II}(H_2O)$_6$](ClO_4)$_2$, 2.122(16) Å[17]}.

The nitrite function in **3** is linked to the metal ion through the nitrogen atom. The Ru−N7 (nitrite−nitrogen) bond distance of 2.034(2) Å is shorter than those observed for other nitroruthenium(II) complexes such as [Ru^{II}(trpy)(arylazopyridine)(NO_2)](ClO_4), 2.057(6) Å;[10] [Ru^{II}(trpy)(PMe_3)$_2$(NO_2)]ClO_4, 2.074(3) Å;[18] and Na_2[Ru(NO_2)$_4$(NO)(OH)], 2.078(3), 2.080(3) Å.[19] The presence of the electron-withdrawing pyridine group of L trans to the NO_2^- function might be responsible for the observed shortening of the Ru−NO_2 bond in **3**. The N−O bond distances of the coordinated NO_2^- are 1.244(3) Å [N7−O1] and 1.257(3) Å [N7−O2]. The O1−N7−O2 angle of 116.9(3)° lies in the range of 113−127°, observed in other transition-metal nitro complexes.[20] The angles involving the two Ru−N−O units are almost identical [Ru−N7−O1, 121.4(2)°; and Ru−N7−O2, 121.7(2)°].

The single crystal of **4** contains acetonitrile and water as solvents of crystallization in the ratio **4**:CH_3CN:H_2O = 1:1:0.5. The Ru−N(nitrosyl) bond length in **4** [Ru−N7, 1.765(12) Å] is relatively shorter than that of the only other structurally characterized ruthenium−terpyridine−nitrosyl complex, [Ru(trpy)(2-phenylpyridine)(NO)]$^{2+}$ [1.826(4) Å].[7] The observed bond shortening in the case of **4** may be due to the trans orientation of the NO function with respect to the electron-withdrawing pyridine ring of L. In the 2-phenylpyridine complex, the NO function is trans to the σ-donating phenyl ligand. The triple bond feature of the N−O bond length [N7−O1, 1.126(14) Å] in combination with the linear mode of Ru−N−O [Ru−N7−O1, 176.2(12)°] signifies the π-acceptor character of the NO^+ ligand in **4**.[7,21]

Intra- and intermolecular C−H···O interactions along with the C−H···π and π···π interactions stabilize the crystal structures of all of the four compounds. The packing diagrams of the crystals reveal that interactions of the type O−H···O, C−H···O, O−H···Cl, C−H···Cl, C−H···N, N−H···O, and N−H···Cl exist in the complexes [Supporting Information (Table S1 and Figure S1)].

The ν_{NO} stretching frequency of **4** appeared at 1945 cm^{-1} as a strong and sharp band. The ν_{NO} stretching frequency value of **4** is much higher than those observed in analogue {Ru(trpy)(NO)(L)} complexes incorporating L = the σ-donating ancillary ligands, 2-phenylpyridine (1858 cm^{-1})[7] and acetylacetonate (1914 cm^{-1}),[8] but lower than those in the π-acidic ligands, bipyridine (1953 cm^{-1})[9] and 2-phenylazopyridine (1960 cm^{-1}).[10]

The ^{1}H NMR spectra of **1**−**4** in $(CD_3)_2SO$ displayed the

(13) Sheu, J. T.; Lin, C. C.; Chao, I.; Wang, C. C.; Peng, S. M. *Chem. Commun*. **1996**, 315.
(14) Facchinetti, A.; Marsich, N.; Camus, A.; Ugozzoli, F.; Massera, C.; Lanfredi, A. M. M. *Inorg. Chim. Acta* **2001**, *324*, 162.
(15) Boelrijk, A. E. M.; Reedijk, J. *J. Mol. Catal.* **1994**, *89*, 63.
(16) Mondal, B.; Walawalkar, M. G.; Lahiri, G. K. *J. Chem. Soc., Dalton Trans*. **2000**, 4209.
(17) Bernhard, P.; Burgi, H. B.; Hauser, J.; Lehmann, H.; Ludi, A. *Inorg. Chem*. **1982**, *21*, 3936.
(18) Leising, R. A.; Kubow, S. A.; Churchill, M. R.; Buttrey, L. A.; Ziller, J. W.; Takeuchi, K. J. *Inorg. Chem*. **1990**, *29*, 1306.
(19) Seddon, E. A.; Seddon, K. R. *The Chemistry of Ruthenium*; Elsevier: New York, 1984.
(20) (a) Simonsen, S. H.; Mueller, M. H. *J. Inorg. Nucl. Chem*. **1965**, *27*, 309. (b) Clark, G. R.; Waters, J. M.; Whittle, K. R. *J. Chem. Soc., Dalton Trans*. **1975**, 2556.
(21) Richter-Addo, G. B.; Wheeler, R. A.; Hixson, A.; Chen, L.; Khan, M. A.; Ellison, M. K.; Schulz, C. E.; Scheidt, W. R. *J. Am. Chem. Soc*. **2001**, *123*, 6314.

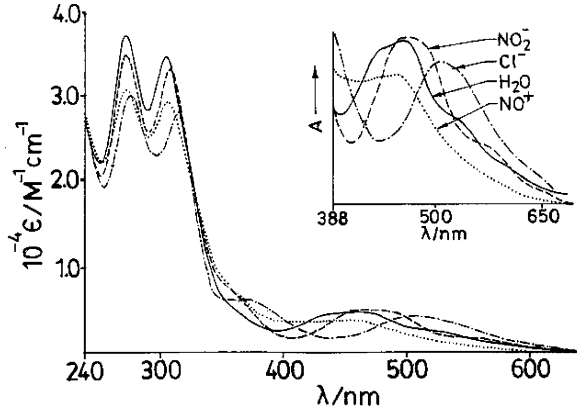

Figure 5. Electronic spectra in acetonitrile of **1** (−•−), **2** (—), **3** (− −), and **4** (···). The inset shows the expanded part of the spectra in the range of 650−388 nm.

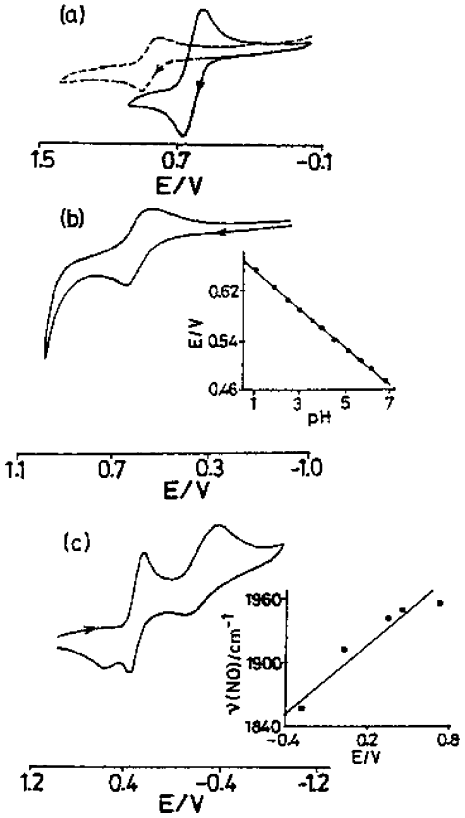

Figure 6. Cyclic voltammograms of (a) **1** (—) and **3** (− −) in CH_3CN; (b) **2** in water at pH = 1.0 (inset shows the variation of the Ru^{IV}/Ru^{II} couple with pH in water); (c) **4** in CH_3CN (inset shows the plot of potentials of the $Ru(NO^+) \rightarrow Ru(NO)$ couple versus the ν_{NO} of five related complexes, as stated in the text).

calculated number of 19 overlapping aromatic protons in each case, occupying between 6.5 and 9.5 ppm, 11 for the terpyridine group and 8 from the dipyridylamine ligand. The NH proton of the coordinated L appeared at 10.45, 10.6, 10.55, and 11.78 ppm for **1**−**4**, respectively, which as expected disappeared during D_2O exchange. The π-acidic character of the NO function makes the NH proton in **4** relatively more acidic, which has been reflected in its downfield chemical shift.

The Ru(II)-based metal-to-ligand charge transfer (MLCT) and ligand-based multiple transitions appeared near 500 nm and in the UV region, respectively (see the Experimental Section, Figure 5). The MLCT band energy in acetonitrile follows the order $Cl^- < NO_2^- < H_2O < NO^+$, depending on the relative stabilization of the dπ(Ru) level. The 35 nm shift in the MLCT band energy, while moving from $[Ru^{II}(trpy)(L)(NO_2)]^+$ (495 nm) to $[Ru^{II}(trpy)(L)(NO)]^{3+}$ (460 nm), is much less than those observed for similar complexes having L = 2-phenylazopyridine (~150 nm)[10] and bipyridine (~130 nm)[9] ligands. This relatively weaker d$\pi(Ru^{II}) \rightarrow \pi^*(NO^+)$ back-bonding implies the lesser electrophilic character of NO^+ in **4** as compared to that of the 2-phenylazopyridine and bipyridine complexes. This has also been reflected in their ν_{NO} stretching frequencies. However, the desirable correlation between the IR/electronic spectral data and the Ru−N(NO)/N−O bond lengths for the known set of analogous $[Ru(trpy)L(NO)]^{3+}$ derivatives has not been possible to derive because the structural details of all of the derivatives are yet to be established.

The plot of absorbance versus pH for **1** and **3** yielded the pK_a values of 9.8 and 9.0, respectively, whereas the same plot for the aqua derivative **2** revealed the presence of two close pK_a values of 9.4 and 10.3 [Supporting Information (Figure S2)] because of the successive dissociations of the OH_2 and NH protons, respectively. The pK_a values of similar ruthenium(II)−monoterpyridine−aqua complexes incorporating 2,2′-bipyridine, 1,10-phenanthroline, 2-phenylazopyridine, 2,2′-bipyrazine, 3,6-di(pyrid-2-yl)pyridazine, and tetramethylenediamine are reported to be 9.7, 9.6, 8.8, 10.3, 10.2, and 7.9, respectively.[22] Thus, as far as the acidity of the coordinated aqua molecule is concerned, **2** is the closest to the bipyridine or phenanthroline derivative. The pK_a value of the nitroso complex **4** was not determined because when it came into contact with a base, it started transforming to the nitro derivative.

The complexes **1** and **3** exhibited one reversible Ru(III)/Ru(II) couple each in acetonitrile at E°_{298}, V (ΔE_p, mV) of 0.64 (80) and 0.88 (80) versus SCE, respectively (Figure 6a), implying a relatively better stabilization of the Ru(II) state in the presence of a stronger electron-withdrawing NO_2^- ligand. The Ru(II) state in **1** or **3** is expectedly less stable compared to the analogous complexes $[(trpy)Ru(L)Cl/NO_2]^+$ where L = stronger π-acidic ancillary ligands bipyridine (Cl^-, 0.81 V; NO_2^-, 1.05 V),[9] 2-phenylazopyridine (Cl^-, 1.07 V; NO_2^-, 1.39 V),[10] 3,6-di(pyrid-2-yl)pyridazine (Cl^-, 0.89 V),[12] bipyrazine (Cl^-, 1.07 V),[12] and *cis*-1,2-bis(diphenylphosphino)ethylene (Cl^-, 1.23 V)[8] but is more stable in comparison to L = σ-donating acetylacetonate (Cl^-, 0.26 V; NO_2^-, 0.42 V)[8] or 2-phenylpyridine (Cl^-, 0.21 V).[7]

The aqua complex $[Ru^{II}(trpy)(L)(H_2O)]^{2+}$ exhibited one quasi-reversible Ru(III)/Ru(II) couple at E°_{298}, V (ΔE_p, mV) of 0.48 (100) in water, and the potential increased linearly with the decrease in pH (Figure 6b). The electron−proton content of the redox process over the pH range of 6.8−1.0 was determined from the slope of the $E_{1/2}$ versus pH plot and in relation with the Nernst equation $E_{1/2} = E_{1/2}^\circ -$

(22) Chanda, N.; Mondal, B.; Puranik, V. G.; Lahiri, G. K. *Polyhedron* **2002**, *21*, 2033.

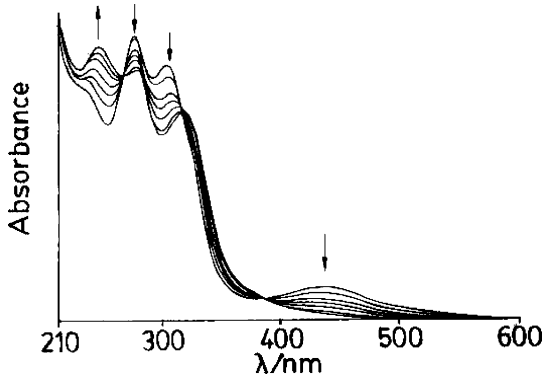

Figure 7. Changes in absorbance of **2** as a function of [Ce(IV)] in 1 N H_2SO_4. The arrows indicate an increase or decrease in band intensities as the reaction proceeds.

(0.059*m*/*n*)pH, where *m* is the number of protons, *n* is the number of electrons, and $E_{1/2}°$ is the half-wave potential at pH = 0.[23] The observed 30 mV change in $E_{1/2}$ per pH unit (Figure 6b) is consistent with the net loss of one proton during the two-electron oxidation process. The two-electron nature of the oxidation process was confirmed by spectrophotometric titration of **2** using an aqueous Ce^{IV} solution in 1 N H_2SO_4. On progressive addition of the acidic Ce^{IV} solution, the intensity of the MLCT band of **2** at 445 nm was found to decrease systematically with the concomitant growth of a new band at a much higher energy (318 nm), and the transformation proceeded with well-defined isobestic points (Figure 7). The plot of the decrease in absorbance of the MLCT band of **2** versus [Ce^{IV}]/**2** showed that a 2:1 mole ratio of Ce^{IV}/**2** was needed for the complete oxidation of the aqua species. The two-electron chemical oxidation process as well as the appearance of a new band at a much higher energy (318 nm) provides direct evidence in favor of the formation of the oxo species $[Ru^{IV}(trpy)(L)(O)]^{2+}$ via the concerted $2e^-/2H^+$ oxidation of **2**. However, the electrochemical results of the net $2e^-/H^+$ transfer during the proton-coupled oxidation process of **2** (as stated above), instead of the expected $2e^-/2H^+$ or stepwise e^-/H^+ processes required for conversion of $Ru^{II}-OH_2$ to $Ru^{IV}=O$, is not clear. The simultaneous selective internal association of one of the liberated protons could be considered as a probable rationale. It may be noted that the bipyridine analogue exhibited two-step processes in the acidic region, $Ru^{II}-H_2O \rightarrow Ru^{III}-OH + e^- + H^+$ and $Ru^{III}-OH \rightarrow Ru^{IV}=O + e^- + H^+$,[24] but bipyrazine,[12] azopyridine,[16] and 3,6-di(pyrid-2-yl)pyridazine[12] analogues showed a concerted $2e^-/2H^+$ process ($Ru^{II}-H_2O \rightarrow Ru^{IV}=O + 2e^- + 2H^+$).

The two successive reductions of the coordinated nitrosyl function of **4** appeared at $E°_{298}$, V (ΔE_p, mV) of 0.34 (80) and −0.34 (irreversible) (Figure 6c), which correspond to $[Ru^{II}(trpy)(L)(NO^+)]^{3+} \rightarrow [Ru^{II}(trpy)(L)(NO^\bullet)]^{2+}$ and $[Ru^{II}(trpy)(L)(NO^\bullet)]^{2+} \rightarrow [Ru^{II}(trpy)(L)(NO^-)]^+$, respectively.[7−10] The corresponding L = 2-phenylazopyridine,[10] bipyridine,[9] acetylacetonate,[8] and 2-phenylpyridine[7] complexes exhibited the mentioned two-step reduction processes at 0.72, 0.07 V; 0.45, −0.20 V; 0.02, −0.75 V; and −0.275 V, respectively. Therefore, a negative shift of the reduction potentials of coordinated NO^+ has taken place during the switching from an environment of 2-phenylazopyridine to bipyridine to dipyridylamine to acetylacetonate to 2-phenylpyridine, depending on their electronic nature. Consequently, the plot of $E_{1/2}$ of the $Ru-NO^+/Ru-NO^\bullet$ couple versus ν_{NO} for the five aforementioned ruthenium−terpyridine−nitrosyl complexes yielded a linear relationship (Figure 6c) because the sensitivity of the $NO^{+/0}$ couple depends on the π-donor ability of the metal ion to the π-acceptor NO^+.

The reductions of the coordinated terpyridine ligands in **1**, **3**, and **4** were also observed at $E°_{298}$, V (ΔE_p, mV) of −1.60 (100), −1.65 (90) and −1.57 (70), and −1.64 (70), respectively.

The electrochemically generated one-electron-reduced species $[Ru^{II}(trpy)(L)(NO^\bullet)]^{2+}$ in acetonitrile exhibited a free-radical electron paramagnetic resonance (EPR) signal (g = 1.990) at 77 K with nitrogen hyperfine structures, which essentially signifies the nitrosyl-based reduction [Supporting Information (Figure S3)].[25] Although the first reduction process $Ru-NO^+ \rightarrow Ru-NO^\bullet$ is reversible and stable on the coulometric time scale, the $Ru-NO^\bullet \rightarrow Ru-NO^-$ process is irreversible even on the cyclic voltammetric time scale, which had essentially prevented any further characterization.

The NO stretching frequency of the electrochemically generated $Ru-NO^\bullet$ species in acetonitrile appeared at 1830 cm^{-1} [Supporting Information (Figure S4)]. The 115 cm^{-1} lowering in the NO stretching frequency, while moving from $Ru-NO^+$ to $Ru-NO^\bullet$, indicates the decrease in bond order of the NO function in the $Ru-NO^\bullet$ species because of a bent $Ru-N-O^\bullet$ geometry.[26]

The nitrosyl complex **4** was found to be stable in the solid state; however, in an aqueous medium, it slowly transformed to the nitro derivative. The rate of conversion of nitroso **4** to nitro **3** {$[Ru^{II}(trpy)(L)(NO)]^{3+} + H_2O \rightarrow [Ru^{II}(trpy)(L)(NO_2)]^+ + 2H^+$} was monitored spectrophotometrically at 298 K in water. The well-defined isobestic points [Supporting Information (Figure S5)] suggest the presence of nitrosyl and nitro complexes in appreciable concentrations during the conversion process. The pseudo-first-order rate constant value (k) at 298 K was calculated to be $k_{298}/s^{-1} = 1.7 \times 10^{-4}$.

In the EtOH/MeOH (4:1) mixture at 77 K, the complex **1** exhibited two distinct emission peaks at 650 and 715 nm (Figure 8a). This is qualitatively similar to the emission spectra reported for the other mixed ligand chelates involving the dipyridylamine ligand, $[Ru^{II}(bpy)(L)_2]^{2+}$, $[Ru^{II}(bpy)_2(L)]^{2+}$, $[Ru^{II}(L)_2(L^-)]^+$, and $Ru^{II}(L^-)_2(L)$.[27] However, in the

(23) Bard, A. J.; Faulkner, L. R. *Electrochemical Methods*; Wiley: New York, 1980; p 213.
(24) Takeuchi, K. J.; Thompson, M. S.; Pipes, D. W.; Meyer, T. J. *Inorg. Chem.* **1984**, *23*, 1845.
(25) (a) de Souza, V. R.; da Costa Ferreira, A. M.; Toma, H. E. *Dalton Trans.* **2003**, 458. (b) McGarvey, B. R.; Ferro, A. A.; Tfouni, E.; Bezerra, C. W. D.; Bagatin, I. A.; Franco, D. W. *Inorg. Chem.* **2000**, *39*, 3577. (c) Callahan, R. W.; Meyer, T. J. *Inorg. Chem.* **1977**, *16*, 574. (d) Diversi, P.; Fontani, M.; Fuligni, M.; Laschi, F.; Marchetti, F.; Matteoni, S.; Pinzino, C.; Zanello, P. *J. Organomet. Chem.* **2003**, *675*, 21.
(26) (a) Haymore, B. L.; Ibers, J. A. *Inorg. Chem.* **1975**, *14*, 3060. (b) Gaughan, A. P.; Haymore, B. L.; Ibers, J. A.; Myers, W. H.; Nappier, T. F.; Meek, D. W. *J. Am. Chem. Soc.* **1973**, *95*, 6859. (c) Pandey, K. K. *Coord. Chem. Rev.* **1992**, *121*, 1.

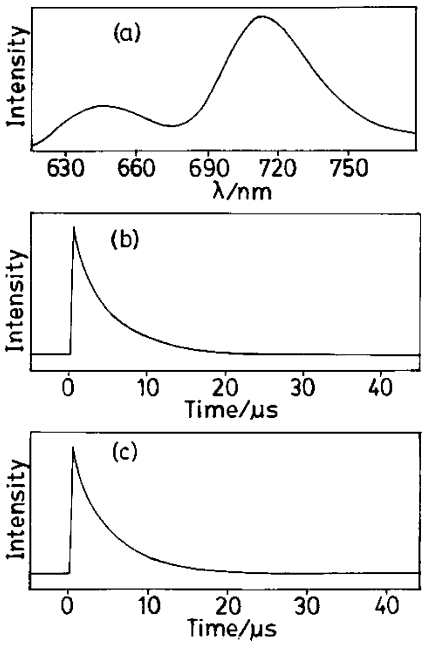

Figure 8. (a) Emission spectrum of **1** in 4:1 EtOH/MeOH glass at 77 K, $\lambda_{ex} = 500$ nm. The time-resolved emission decays of **1** in 4:1 EtOH/MeOH glass at 77 K, λ_{em} at (b) 725 nm and (c) 625 nm, $\lambda_{ex} = 532$ nm.

case of **1**, the emission peaks are better resolved as compared to those of the earlier systems. During the excitation by millijoule pulses of the 532 nm laser, the emission decays were found to exhibit a dependence on the wavelength of emission, and the decays at 625 and 725 nm are shown in parts b and c of Figure 8, respectively. The best fits of the decay curves revealed the biexponential functions. A component of ca. 1 μs is present in both of the traces. Its contribution is 96% at 725 nm, whereas it is 50% at 625 nm. The second component has a value of 6 μs. These steady-state and time-resolved emission results clearly indicate the presence of two sources of emission. The longer-lived and shorter-lived ones predominate at 625 and 725 nm, respectively. In the absence of the heterogeneity in the ground state, we suggest that the dual emission arises because of the involvement of two kinds of excited states. Though a detailed photophysical study including emission as well as transient absorption experiments is needed to get a precise understanding of the origin of this dual emission, a tentative assignment can be made based on the earlier results related to other Ru−L complexes, which show dual emission separated in energy as well as time, as reported by DeArmond and co-workers.[27] The problem with obtaining a bona fide dual emission from the Ru(II) complexes has also been discussed earlier by Balzani and von Zelewsky.[28] If the spectroscopic properties of the two ligands in a mixed-ligand complex are sufficiently different, then it is expected that the nonradiative transition from the higher to the lower energy ligand would precede the emission and, hence, no dual emission would be expected. However, it is well established that the optical orbitals of the emitting states for many of these complexes are localized over single chelate rings, rather than being delocalized over the entire complex. In such cases, the lack of interligand interactions would hinder, if not obliterate, such a nonradiative transition, and so a dual emission could be expected.

(27) (a) Blakley, R. L.; DeArmond, M. K. *J. Am. Chem. Soc.* **1987**, *109*, 4895. (b) Blakley, R. L.; Myrick, M. L.; DeArmond, M. K. *J. Am. Chem. Soc.* **1986**, *108*, 7843. (c) Morris, D. E.; Ohsawa, Y.; Segers, D. P.; DeArmond, M. K.; Hanck, K. W. *Inorg. Chem.* **1984**, *23*, 3010. (d) Segers, D. P.; DeArmond, M. K. *J. Phys. Chem.* **1982**, *86*, 3768.

(28) (a) Belser, P.; von Zelewsky, A.; Juris, A.; Barigelletti, F.; Balzani, V. *Chem. Phys. Lett.* **1984**, *104*, 100. (b) Cocks, A. T.; Wright, R.; Seddon, K. R. *Chem. Phys. Lett.* **1982**, *85*, 369.

Conclusion

The present paper illustrates the following important features: (i) the complexes **1**−**4** represent the first example of structurally characterized ruthenium−dipyridylamine systems where the dipyridylamine ligand functions as a terminal bidentate ligand; (ii) the chloro complex **1** exhibits dual luminescence at 650 and 715 nm with excited-state lifetimes of 6 and 1 μs, respectively; (iii) the oxidation of aqua complex **2** by acidic Ce^{IV} ion results in the corresponding oxo derivative $[Ru^{IV}(trpy)(L)(O)]^{2+}$, via the concerted $2e^-/2H^+$ oxidation process; (iv) the selective combination of 2,2′-dipyridylamine with the terpyridine function in **4** yields a coordinated nitrosyl center with a linear Ru−N−O feature [Ru−N−O, 176.2(12)°] and high ν_{NO} stretching frequency of 1945 cm^{-1}; (v) the nitrosyl complex **4** is reasonably stable in aqueous solution and only slowly transforms to the corresponding nitro derivative **3**; (vi) the free-radical EPR spectrum of the reduced species $[Ru^{II}(trpy)(L)(NO^{\bullet})]^{2+}$ suggests that the unpaired electron is preferentially localized on the nitrosyl center; (vii) the 115 cm^{-1} lowering of the NO stretching frequency during the moving from $Ru-NO^+$ to $Ru-NO^{\bullet}$ implies the change in the linear $Ru-NO^+$ mode to the bent $Ru-NO^{\bullet}$ geometry.

Experimental Section

The precursor complex $Ru^{III}(trpy)Cl_3$ was prepared as reported.[12d] 2,2′-Dipyridylamine was purchased from Aldrich. Other chemicals and solvents were reagent grade and used as received. For spectroscopic and electrochemical studies, HPLC-grade solvents were used. Water of high purity was obtained by distillation of deionized water from $KMnO_4$ under a dinitrogen atmosphere. The electrical conductivity of the solution was checked using a Systronic conductivity bridge 305. Infrared spectra were taken on a Nicolet spectrophotometer with samples prepared as KBr pellets, and far-IR spectra were recorded with samples prepared as polyethylene disks. ^1H NMR spectra were recorded for the $(CD_3)_2SO$ solutions using a 400 MHz Varian FT spectrometer. UV−vis spectral studies were performed on a Jasco-570 spectrophotometer. Cyclic voltammetric and coulometric measurements were carried out using a PAR model 273A electrochemistry system. A platinum wire working electrode, platinum wire auxiliary electrode, and saturated calomel reference electrode were used in a standard three-electrode configuration. Tetraethylammonium perchlorate was the supporting electrolyte, and the solution concentration was ca. 10^{-3} M; the scan rate used was 50 mV s^{-1}. A platinum gauze working electrode was used in the coulometric experiments. All of the electrochemical experiments were carried out under a dinitrogen atmosphere, and all of the redox potentials are uncorrected for junction potentials. The EPR measurements were made with a Varian model 109C E-line X-band spectrometer fitted with a quartz Dewar for measurements at 77 K. The elemental analyses were carried out with a

Perkin-Elmer 240C elemental analyzer. Electrospray mass spectra were recorded on a Micromass Q-TOF mass spectrometer. Steady-state emission experiments were made using a Perkin-Elmer LS 55 luminescence spectrometer fitted with a cryostat. The time-resolved fluorescence data were obtained by exciting the sample by millijoule pulses of the third harmonic (532 nm) of a picosecond-pulsed Continuum Nd:YAG laser operating at 5 Hz. For the determination of k of the conversion process $[Ru^{II}(trpy)(L)(NO)]^{3+} \rightarrow [Ru^{II}(trpy)(L)(NO_2)]^{+}$ in water, the increase in absorbance (A_t) at 449 nm corresponding to the λ_{max} of the nitro complex was recorded as a function of time (t). A_α was measured when the intensity changes leveled off. Values of the pseudo-first-order rate constants (k) were obtained from the slopes of the linear least-squares plots of $-\ln(A_\alpha - A_t)$ against t.[29]

Synthesis of 1. Starting complex $[Ru^{III}(trpy)Cl_3]$ (100 mg, 0.23 mmol), 2,2′-dipyridylamine ligand (L, 47 mg, 0.28 mmol), excess LiCl (54 mg, 1.3 mmol), and NEt_3 (0.4 mL) were taken in 15 mL of ethanol, and the mixture was heated at reflux for 2.5 h under a dinitrogen atmosphere. The initial dark brown color of the solution gradually changed to a deep purple. The solvent was then removed under reduced pressure. The dry mass was dissolved in a minimum volume of acetonitrile, and an excess saturated aqueous solution of $NaClO_4$ was added to it. The solid precipitate thus obtained was filtered off and washed thoroughly by cold ethanol followed by ice-cold water. The product was dried in vacuo over P_4O_{10}. It was then purified by using an alumina (neutral) column. The complex **1** was eluted by 5:3 CH_2Cl_2/CH_3CN. Evaporation of the solvent under reduced pressure afforded the pure complex **1**. Yield: 102 mg (70%). Anal. Calcd (found): C, 46.89 (47.24); H, 3.15 (3.29); N, 13.12 (13.49). Molar conductivity [Λ_M (Ω^{-1} cm^2 M^{-1})] in acetonitrile: 135. λ_{max}/nm (ϵ/M^{-1} cm^{-1}) in acetonitrile: 506 (4280), 318 (27 720), 278 (30 060), 238 (27 200), and 208 (22 450). The positive ion electrospray mass spectrum in acetonitrile showed the molecular ion peak centered at $m/z = 541$ [Supporting Information (Figure S6)] corresponding to $[\mathbf{1}-ClO_4]^+$ (calculated molecular mass: 541.04).

Synthesis of 2. The chloro complex **1** (100 mg, 0.16 mmol) was taken in 25 mL of water and heated at reflux for 5 min. An excess of $AgNO_3$ (265 mg, 1.56 mmol) was added to the above hot solution, and the heating was continued for 1 h. It was then cooled, and the precipitated AgCl was separated by filtration through a sintered glass crucible (G-4). The volume of the filtrate was reduced to 10 mL, and a saturated aqueous $NaClO_4$ solution was added. The solid aqua complex **2** thus obtained was filtered off, washed with ice-cold water, and dried in vacuo over P_4O_{10}. Yield: 100 mg (89%). Anal. Calcd (found): C, 41.56 (41.18); H, 3.07 (3.13); N, 11.63 (11.88). Molar conductivity [Λ_M (Ω^{-1} cm^2 M^{-1})] in acetonitrile: 220. λ_{max}/nm (ϵ/M^{-1} cm^{-1}) in acetonitrile: 472 (4860), 308 (34 810), 276 (37 260), and 216 (32 520). The positive ion electrospray mass spectrum in acetonitrile showed the molecular ion peak centered at $m/z = 605.17$ [Supporting Information (Figure S6)] corresponding to $[\mathbf{2}-H_2O-ClO_4]^+$ (calculated molecular mass: 605.02).

Synthesis of 3. The aqua complex **2** (100 mg, 0.14 mmol) was dissolved in 25 mL of hot water, and an excess of $NaNO_2$ (94 mg, 1.37 mmol) was added to it. The mixture was heated at reflux for 1 h. The light brown solution of the aqua species changed to orange during the course of reaction. The pure crystalline nitro complex was precipitated out when the hot solution cooled to room temperature. The solid mass thus obtained was filtered off, washed with ice-cold water, and dried in vacuo over P_4O_{10}. Yield: 76.6 mg (85%). Anal. Calcd (found): C, 46.13 (45.75); H, 3.10 (3.00); N, 15.06 (15.53). Molar conductivity [Λ_M (Ω^{-1} cm^2 M^{-1})] in acetonitrile: 140. λ_{max}/nm (ϵ/M^{-1} cm^{-1}) in acetonitrile: 495 (4680), 313 (33 120), 274 (35 280), 233 (31 120), and 199 (56 100). The positive ion electrospray mass spectrum in acetonitrile showed the molecular ion peak centered at $m/z = 552.18$ [Supporting Information (Figure S6)] corresponding to $[\mathbf{3}-ClO_4]^+$ (calculated molecular mass: 552.07).

Synthesis of 4. Concentrated HNO_3 (2 mL) was added dropwise directly to the solid nitro complex **3** (100 mg, 0.15 mmol) at 273 K under a stirring condition. To the pasty mass thus formed was added ice-cold concentrated $HClO_4$ (6 mL) dropwise with continuous stirring by using a glass rod. A yellow solid product was formed during the addition of a saturated aqueous $NaClO_4$ solution. The precipitate was filtered off immediately, washed with a little ice-cold water, and then dried in vacuo over P_4O_{10}. Yield: 115 mg (90%). Anal. Calcd (found): C, 36.01 (35.70); H, 2.42 (2.47); N, 11.76 (11.99). Molar conductivity [Λ_M (Ω^{-1} cm^2 M^{-1})] in acetonitrile: 365. λ_{max}/nm (ϵ/M^{-1} cm^{-1}) in acetonitrile: 460 (3600), 312 (29 340), and 275 (31 032). The positive ion electrospray mass spectrum in acetonitrile showed the molecular ion peak centered at $m/z = 634.04$ [Supporting Information (Figure S6)] corresponding to [**4** incorporating $NO^{\bullet}-ClO_4]^+$ (calculated molecular mass: 635.02).

Crystal Structure Determination. Single crystals of **1**, **3**, and **4** were grown by the slow diffusion of an acetonitrile solution of the complex in benzene followed by slow evaporation. The single crystals of **2** were grown by the slow evaporation of an aqueous solution of complex **2**. The data for **1** were collected at 173 K using a Siemens P3 diffractometer. The data of complex **2** were collected on a Bruker SMART APEX CCD diffractometer at 293 K. The data for **3** and **4** were collected at 293 K on a Enraf−Nonius CAD-4 (MACH-3) diffractometer. Selected data collection parameters and other crystallographic data are summarized in Table 2. Calculations were carried out with the SHELXTL PC 5.03[30] and SHELXL-97[31] program systems installed on local personal computers. The phase problem was solved by direct methods, and the structure was refined on F_o^2 by the full-matrix least-squares refinement. An absorption correction was applied by using semiempirical Ψ scans. Anisotropic thermal parameters were refined for all of the nonhydrogen atoms. Hydrogen atoms were placed in idealized positions and refined in riding model approximations with a common isotropic displacement parameter. X-ray analysis revealed the presence of a quarter of a water molecule as the solvent of crystallization in **2** and in **4** three disordered ClO_4^- ions and one acetonitrile molecule along with half of a water molecule as the solvents of crystallization in the asymmetric units, respectively.

Acknowledgment. We thank the Council of Scientific and Industrial Research, New Delhi, India, for financial support. The X-ray structural studies for the complexes **3** and **4** were carried out at the National Single Crystal Diffractometer Facility, Indian Institute of Technology, Bombay, India. Special acknowledgment is made to the Sophisticated Analytical Instrument Facility, Indian Institute of Technology, Bombay, India, for providing the EPR and far-IR facilities. We thank Dr. Dilip Kumar Palit, Bhabha

(29) Wilkins, R. G. *The Study of Kinetics and Mechanism of Reactions of Transition Metal Complexes*; Allyn and Bacon, Inc.: Boston, MA, 1974.

(30) *SHELXTL PC 5.03*; Siemens Analytical X-ray Instruments Inc.: Madison, WI, 1994.

(31) Sheldrick, G. M. *Program for Crystal Structure Solution and Refinement*; Universität Göttingen: Göttingen, Germany, 1997.

Atomic Research Center, Trombay, India, for the time-resolved data.

Supporting Information Available: X-ray crystallographic data for the complexes **1**−**4** in CIF format; hydrogen bonds and short contacts in **1**−**4** (Table S1); packing diagrams of **1**−**4** (Figure S1); UV−vis spectra of **2** in the pH range of 6−12 (Figure S2); EPR spectrum of $[Ru^{II}(trpy)(L)(NO^{\bullet})]^{2+}$ (Figure S3); FTIR spectra of **4** and $[Ru^{II}(trpy)(L)(NO^{\bullet})]^{2+}$ (Figure S4); electronic spectra of a changing solution of **4** → **3** at 298 K (Figure S5); and electrospray mass spectra of **1**−**4** (Figure S6). This material is available free of charge via the Internet at http://pubs.acs.org.

IC034902N